Modelling and Measurements of the Microwave Dielectric Properties of Microspheres

Ali A. Abduljabar, *Student Member, IEEE*, Xin Yang, David A. Barrow, and Adrian Porch

***Abstract*—A microwave microstrip sensor incorporating a split ring resonator is presented in this paper for microsphere detection and dielectric characterization within a microfluidic channel. Split ring resonator (SRR) sensor of three different radii, but with approximately equal gap dimensions to change their sensitivity, were designed and fabricated, of resonance frequencies 2.5, 5.0 and 7.5 GHz. To validate the SRR sensors, two sizes of polystyrene microspheres were tested, of diameters 15 and 25 μm. Measurements of changes in resonance frequency and insertion loss of the odd SRR mode were related to the dielectric contrast provided by the microspheres and their host solvent, here water. COMSOL Multiphysics was used to model the sensors, and good agreements were found between the simulated and measured results.**

***Index Terms*—Cell detection, microspheres, microwave sensor, split ring resonator.**

I. Introduction

MUCH research has been undertaken in the use of microwave methods for the realization of rapid, reliable, accurate and non-invasive bio-sensors. Recent use of microwave methods for detecting the dielectric properties of human cells has yielded compelling results [1]. The dielectric property of a single cell has also been investigated by using a microwave biosensor [2], incorporating a capacitive sensing zone for trapped cells within microfluidic channel. Microwave dielectric spectroscopy has been identified as a promising method to study the membrane permeabilization of cells induced by chemo-treatment, and its consequences for the cells [3]. An original label free bio-sensing approach for cellular study based on micro-technologies at RF frequencies is also proposed [4]. This bio-detection method presents advantages in that it is label free and of sub-millimetric size, allowing operation at the cell scale and with a limited number of cells. A tuneable, resonant, microwave biosensor that allows measurement of the dielectric permittivity of microscale particles over a range of frequencies is presented in [5]. A cost-effective, scalable microwave system that can be integrated with microfluidic devices enabling remote, simultaneous sensing and heating of individual nanoliter-sized droplets generated in microchannels is proposed in [6]. A new type of biosensor based on a two pole microstrip filter, using the inter-resonator's planar coupling capacitor as an ultrasensitive biosensing element, has been developed to investigate the electrical parameters of human cells [7].

A method to measure the permittivity of single particles and yeast cells at microwave frequencies is presented in [8] and [9], respectively. An electrical approach for single-cell analysis, wherein a 1.6 GHz microwave interferometer detects the capacitance changes produced by single cells flowing past a coplanar interdigitated electrode pair, is demonstrated in [10]. A passive microwave sensor based on microstrip lines for characterizing cell cultivation in aqueous compartments is presented in [11]. The cultivation stadium of a yeast culture was monitored to detect the permittivity changes. In [12] and [13], broadband microwave measurements and sensing of single Jurkat and HEK cells were used to overcome electrode polarization, with ac dielectrophoresis used to precisely place cells between narrowly spaced electrodes, and relatively wide microfluidic channels incorporated to prevent cell clogging.

A miniaturized microwave based biosensor was fabricated in [14] for the characterization of living and dead cells via their dielectric properties. Another detection system is based on a microwave coupled transmission line resonator integrated into an interferometer [15], designed for the detection of biomaterials in a variety of suspending fluids.

However, most of these works have been dedicated to the dielectric assessment of groups of cells, rather than single cell properties. Increasing evidence in other clinical and pre-clinical studies suggests that the single-cell heterogeneity in the regulation of oncogenic signaling pathways is a general feature of most cancers. In [16] it was shown that the dielectric permittivity, capacitance and conductivity values of cell membranes are higher for normal lymphocytes than for malignant ones. Model-based numerical predictions of the dielectrophoretic behavior of spheroidal biological cells are carried out in [17]. A linear relationship was observed between the DNA content of eukaryotic cells and the change in capacitance in [18] that is evoked by the passage of individual cells across a 1-kHz electric field. Moreover, theoretical analysis and measurement techniques for dielectric spectroscopy of biological cells in the radio frequency range were reviewed in [19].

In this work, we demonstrate a new application for a microwave split ring resonator (SRR) with a narrow, tapered gap section, as a sensor for the dielectric characterization of microparticles. This is shown schematically in Fig. 1, illustrating the gap adaption for single cell investigations in medical and

Manuscript received June 05, 2015; revised August 14, 2015 and October 20, 2015; accepted October 20, 2015. Date of publication November 12, 2015; date of current version December 02, 2015. This paper is an expanded version from the IEEE MTT-S International Microwave Symposium, Phoenix, AZ, USA, May 17–22, 2015.

A. A. Abduljabar was with the College of Engineering, University of Basrah, Basrah, Iraq. He is now with the School of Engineering, Cardiff University, Cardiff, CF24 3AA, U.K. (e-mail: abduljabaraa@cardiff.ac.uk).

X. Yang, D. A. Barrow, and A. Porch are with the School of Engineering, Cardiff University, Cardiff, CF24 3AA, U.K. (e-mail: yangx26@cardiff.ac.uk; barrow@cardiff.ac.uk; porcha@cardiff.ac.uk).

Color versions of one or more of the figures in this paper are available online at http://ieeexplore.ieee.org.

Digital Object Identifier 10.1109/TMTT.2015.2495247

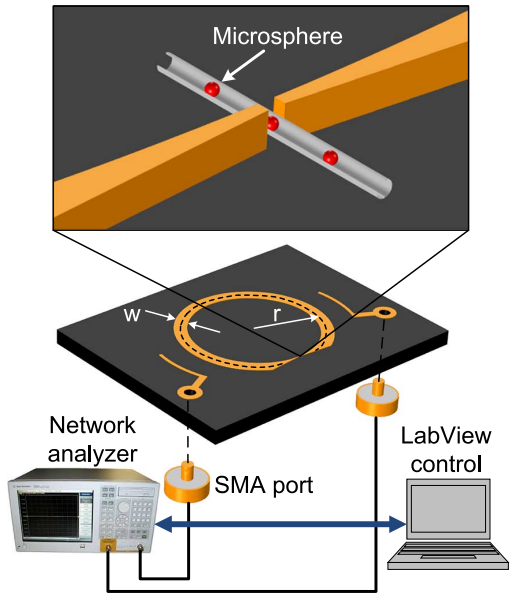

Fig. 1. Schematic of the split-ring microstrip sensor (the ground plane is on the back surface, not shown), connected to a microwave network analyzer and controlled by a LabVIEW program. Microspheres are passed through the gap region via a water filled, glass capillary, after [20].

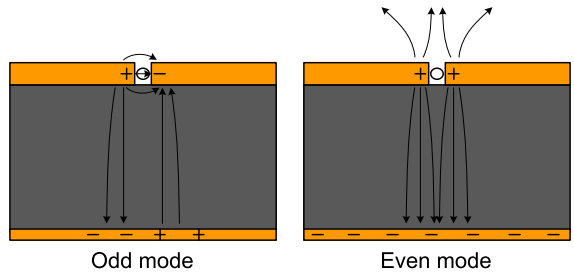

Fig. 2. Quasi-TEM modes of the SSR. (a) Odd mode (with large electric field in the gap), and (b) even mode (with small electric field in the gap).

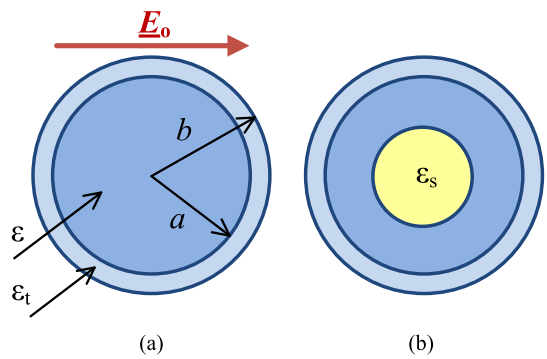

Fig. 3. Cross section of the capillary filled by liquid, (a) without a microsphere, and (b) with a microsphere. The dimensions and relative permittivities of all regions are shown.

biological applications. Three sizes of the sensors are presented in this work, model A, B, and C, where the design and measurements of model A was presented in [20]. The added work of this paper is the miniaturization of model A sensor to models B and C to enhance sensor sensitivity.

In Section II, the theory and concepts of the polarization of the liquid with and without spheres ("cells") are presented; also the theoretical enhancements in sensitivity that can be expected by tapering and reducing the gap, and that due to reducing the overall size of the SRR. A description of the sensor design and fabrication (together with simulation results) are presented in Section III. In Section IV, the experimental results are demonstrated and discussed, with final conclusions described in Section V.

II. Concepts, Theory and Simulation

A. Odd and Even Resonator Modes

The SRR based on the microstrip geometry (i.e., with ground plane) shown in Fig. 1 has odd and even mode resonances. The odd mode has the lower resonance frequency and occurs when the wavelength is equal to the electrical length of the ring plus the gap [21]; the even mode has higher frequency and occurs when the wavelength is equal to the ring length only [22].

The distribution of electric field in the gap cross section for both modes is shown schematically in Fig. 2. In the odd mode configuration the electric field penetrates the gap where the capillary resides, while in even mode the electric field is mostly outside the gap. In our experiments, the odd mode is used to characterize the presence of microspheres whilst the even mode is insensitive to the microspheres but can be used as a useful reference, for example, to account for small changes in temperature.

The input and output power couplings of the resonator are mostly inductive owing to their positioning at a magnetic field antinode, with a smaller degree of capacitive coupling arising from the fact that they are extended structures and are made of open-circuit, microstrip sections [23].

B. Electric Dipole Moment Calculations

Next we develop a simple, approximate theory to account for the change of electric dipole moment of the capillary within the gap when a microsphere is present. This allows us to calculate the resonator perturbation using first order perturbation theory [24] and [25].

Consider first a liquid of complex relative permittivity ε completely filling a low loss tube (for example, glass, as in the experiments here). Referring to Fig. 3(a), we define ε_t as the (real) permittivity of the tube, and b and a to be its outer and inner radii, respectively. The complex electric dipole moment p induced for a length ℓ of a filled tube can be calculated analytically based on the direct solution of Laplace's equation for a quasi-static electric field. The main result is [25]

$$p(\varepsilon) = 2\pi\ell b^2 \left(\frac{(\varepsilon+\varepsilon_t)(\varepsilon_t-1)+\gamma(\varepsilon-\varepsilon_t)(\varepsilon_t+1)}{(\varepsilon+\varepsilon_t)(\varepsilon_t+1)+\gamma(\varepsilon-\varepsilon_t)(\varepsilon_t-1)} \right) \varepsilon_0 E_0 \tag{1}$$

where E_0 is the magnitude of the electric field applied perpendicular to the tube's axis, assumed to be uniform along the length of the tube, and $\gamma = a^2/b^2$.

The perturbations measured experimentally in this paper are due to the presence of polystyrene microspheres within the gap region. Referring to Fig. 3(b), we next analyse quantitatively how the presence of a small spherical particle, assumed to be homogeneous and of relative permittivity ε_s, modifies the electric dipole moment of a water filled tube and so leads to perturbations of the resonator parameters. If the sphere occupies a

volume fraction β of the liquid within the tube (with $\beta \ll 1$), the complex permittivity of the liquid in the tube can be considered to have changed from ε to an effective value $\varepsilon_{\rm eff}$. This is estimated from simple effective medium theory to be

$$\varepsilon_{eff} \approx \varepsilon \left(1 + \frac{3\beta(\varepsilon_s - \varepsilon)}{\varepsilon_s + 2\varepsilon}\right). \tag{2}$$

The resulting perturbation in electric dipole moment is then the difference

$$\Delta p \approx p(\varepsilon_{eff}) - p(\varepsilon). \tag{3}$$

C. Cavity Perturbation Theory

First order cavity perturbation theory states that a small change in electric dipole moment Δp due, for example, to a change in ε will result in changes (i.e., perturbations) in both the resonance frequency f and unloaded quality factor Q, given by the approximate formulae [26]

$$\Delta f = f_1 - f_0 \approx -f_0 \mathrm{Re}\left(\frac{\Delta p\, E_0^*}{4U}\right) \tag{4}$$

$$\Delta\left(\frac{1}{Q}\right) = \frac{1}{Q_1} - \frac{1}{Q_0} \approx -\mathrm{Im}\left(\frac{\Delta p\, E_0^*}{2U}\right). \tag{5}$$

Here the subscripts "1" and "0" denote the perturbed and unperturbed states of the resonator, respectively. The quantity U is the time averaged stored energy of the resonator in its unperturbed state, defined by

$$U = \frac{1}{2}\varepsilon_0 \oint_V E^2 dV \equiv \frac{1}{2}\varepsilon_0 E_0^2 V_m, \quad V_m = \oint_V \frac{E^2}{E_0^2} dV \tag{6}$$

where E_0 is the unperturbed electric field magnitude at the position of the tube and $V_{\rm m}$ is the mode volume of the resonator. This latter term quantifies the concentration enhancement of electric energy density at the position of the tube relative to the average electric energy density elsewhere in the resonator. Miniaturizing the resonator by, for example, reducing the gap width or the ring radius, results in a decreased value of $V_{\rm m}$ and hence also a decreased value of U, thus causing larger changes in resonator parameters for a given perturbation Δp (i.e., enhanced sensitivity to the cause of the perturbation), which we will return to in more detail below.

To gain a better physical understanding of how the presence of a microsphere affects the SRR, for the moment we ignore the presence of the glass tube (assumed to be very thin walled) and develop an approximate formula for Δp in the limit when the permittivity of the host liquid ε is much greater than that of the microsphere $\varepsilon_{\rm s}$. This will indeed be the case when water ($\varepsilon \approx 78 - j12$ at 2.45 GHz) and polystyrene ($\varepsilon_{\rm s} \approx 2.0$) are considered, respectively. Then, (1)–(5) reduce to the very simple results

$$\Delta p \approx -\frac{6\pi\ell a^2 \beta}{\varepsilon}\varepsilon_0 E_0 \tag{7}$$

$$\frac{\Delta f}{f_0} \approx +\frac{3\beta V_{\rm t}}{V_{\rm m}}\mathrm{Re}\left(\frac{1}{\varepsilon}\right) \tag{8}$$

$$\Delta\left(\frac{1}{Q}\right) \approx +\frac{6\beta V_{\rm t}}{V_{\rm m}}\mathrm{Im}\left(\frac{1}{\varepsilon}\right) \tag{9}$$

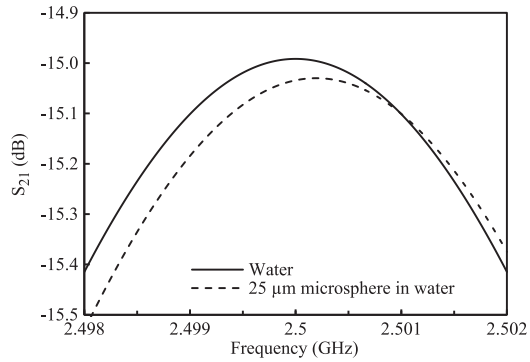

Fig. 4. The calculated transmission spectrum of the SRR with (dotted) and without (solid) a plastic microsphere in the gap region. Both resonance frequency and microwave loss increase with the presence of the sphere. In this calculation, the SRR is assumed to have a Q factor of 200 and a resonance frequency of 2.5 GHz when unperturbed by the microsphere. The microsphere is assumed to occupy a volume fraction of 0.1 of the gap volume, and the ratio of tube volume to mode volume is 0.02. The microsphere permittivity is assumed to be 2 and the water permittivity $78 - j12$. In this limit when $\varepsilon \gg \varepsilon_{\rm s}$, the simplified analysis using (7) for Δp gives almost identical results to the more rigorous analysis using (1)–(3).

where $V_{\rm t} = \pi\ell a^2$ is the physical volume of the sample within the gap region. From this we see that on introducing a polystyrene microsphere into the gap region, the resonance frequency increases, but that the Q factor decreases (i.e., the microwave loss increases). This is illustrated further in Fig. 4, where we consider the effects of the presence of a microsphere on the voltage transmission coefficient S_{21} in the frequency domain, with perturbation calculated using both (1)–(3) and the simplified formula (7).

This can be understood by referring to Fig. 5, where we plot the electric field intensity E^2 in the space in an around a sphere placed in a uniform electric field when (a) the sphere's permittivity is much less than that of its host liquid (as is the case here), and (b) when the sphere's permittivity is much greater than that of its host (as would be the case for a metal sphere). In (a), we note that the intensity is enhanced within the host liquid adjacent to the equatorial regions of the sphere, whilst in (b) it is enhanced adjacent to the polar regions. In both cases, this intensity enhancement increases the overall dielectric loss. However, in (b) there is an increase in electrical potential energy owing to the strong polarisation of the sphere, so the resonance frequency would decrease. In (a), since the sphere is of a low permittivity material, its polarisation is small and overall the electric potential energy is reduced, resulting in an increased resonance frequency.

D. Sensitivity Enhancement of the SRR

It can be seen from the perturbation (4)–(6), and their simplified counterparts (8), (9), that greatest SRR sensitivity to the presence of a single microsphere is attained when its mode volume $V_{\rm m}$ is reduced. This is most easily accomplished by reducing the ring radius r of the SRR. Table I shows the results of a COMSOL Multiphysics 4.4 simulation of the SRR shown in Fig. 1, with varying radii r, giving unperturbed resonance frequencies labelled f_0. As expected, to a good approximation $f_0 \propto 1/r$ since the SRR's lumped inductance L is proportional to the ring area πr^2, and $f_0 \propto 1/\sqrt{L}$. The gap region is 70 μm deep (defined by the thickness of the copper cladding),

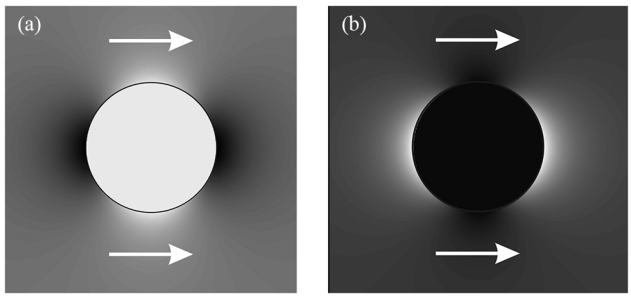

Fig. 5. The calculated electric field intensity E^2 around a sphere when (a) its permittivity is much less than that of its host liquid, and (b) much greater than that of its host (the arrows show the direction of the applied field). The enhancement of E^2 in the host in both cases gives rise to increased losses but in (a) the overall electric potential energy is reduced, giving rise to an increased resonance frequency.

TABLE I
EFFECT OF VARYING SRR DIMENSIONS (SHOWN IN FIG. 1) ON RESONANCE FREQUENCY, Δf, AND EFFECTIVE VOLUME

r (mm)	w (mm)	Frequency, f_0 (GHz)	Δf (MHz)	$\Delta f/f_0$	$V_{\rm m}$ (mm^3)
1.75	0.5	9.8150	2.000	0.000204	0.01301
2.25	0.5	7.4280	1.200	0.000162	0.01641
3.50	1.0	4.9420	0.550	0.000111	0.02382
5.50	1.0	3.9093	0.325	0.0000831	0.03188
7.35	1.3	2.5073	0.150	0.0000598	0.04431

with in-substrate gap widths of 35 μm $\times$ 35 μm to give a total geometrical volume of the gap of 8.58×10^4 μm^3 (i.e., 8.58×10^{-5} mm^3).

We also simulate the perturbation on the SRR region imposed by inserting a single, spherical metal particle of radius 7.5 μm within the gap volume. The sphere volume is 2.1% of the gap volume, thus giving a small perturbation from which the mode volume $V_{\rm m}$ for SRRs of varying radii can be computed using (4). The resulting decrease in resonance frequency Δf is also shown in Table I. A metal sphere of radius a completely depolarises the electric field within it by developing an electric dipole moment $p = 4\pi\varepsilon_0 E_0 a^3 = 3\varepsilon_0 E_0 V_s$, where $V_{\rm s}$ is the volume of the sphere. This means that the mode volume $V_{\rm m}$ can be calculated from Δf of a metal sphere using

$$V_{\rm m} \approx -\frac{3V_{\rm s} f_0}{2\Delta f} \tag{10}$$

The resulting values for $V_{\rm m}$ are also shown in Table I. The fact that $V_{\rm m}$ increases with increasing radius r is indicative of the fact that the electrical energy is not solely stored within the gap region, but occupies a much larger volume outside of the gap. This is associated with charge storage on the curved ring surfaces itself, which is more effective the larger the radius r. The main results of Table I are plotted in Fig. 6, for the resonance frequency f_0 (Fig. 6(a)) and also the mode volume $V_{\rm m}$ (Fig. 6(b)) as a function of ring radius r.

III. DESIGN AND REALIZATION

The SRRs were fabricated by initial cutting of the ring shape and the gap structure using laser micromachining followed by fine finishing with a milling machine. The gap is defined in this way to a tolerance of 1 to 2 micrometer. A Rogers Corporation RT/duroid 5880 laminate was used with a substrate (dielectric) thickness of 1.57 mm, relative permittivity of 2.20 $\pm$ 0.02 and loss tangent 0.0009. The thickness of the copper is 70 μm, which is chosen to be as thick as possible to ensure a higher quality factor Q. Polystyrene microspheres (*Alfa Aesar*, A Johnson Matthey Company) were chosen to validate the sensor, of 15 and 25 μm diameters. These were dispersed in water and passed through the glass micro-capillary with the aid of a syringe.

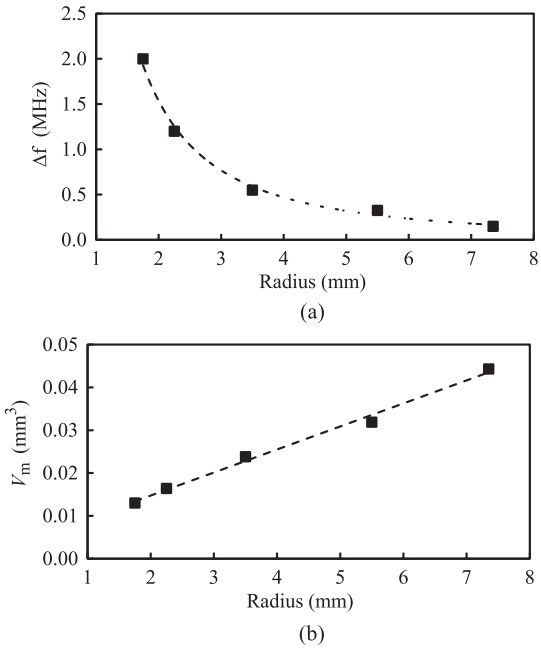

Fig. 6. Simulated results of varying the ring radius r of the SSR. (a) Resonance frequency for different ring radii. (b) Effective volume for different ring radii (assuming a constant gap geometry).

TABLE II
DIMENSIONS OF THE SPLIT RING RESONATORS SHOWN IN FIG. 7, ALL DIMENSIONS ARE IN MM

Model	r_1	r_2	r_3	r_4	ℓ	gap
A	10.9	10.6	8.0	6.7	6.0	0.035
B	6.6	6.3	4.0	3.0	3.0	0.030
C	4.6	4.4	2.5	2.0	1.5	0.030

Three sizes of SRRs were designed to study the effect of the ring radius on the microsphere detection, here denoted models A, B and C; their dimensions are listed in Table II. By changing the dimensions we change the mode volume $V_{\rm m}$, which reduces in going from model A to B to C, thus increasing their sensitivity to microsphere detection. In model A the gap was designed to be of width 35 μm, which is wide enough for two sizes of microsphere (diameters 25 and 15 μm) to pass through it, while in models B and C the gap and radius were reduced to increase the detection sensitivity of the smaller microspheres (diameter 15 μm).

The soda glass capillary (SAMCO company) with permittivity of 3.8, inner diameter of 1.3 mm, and outer diameter of

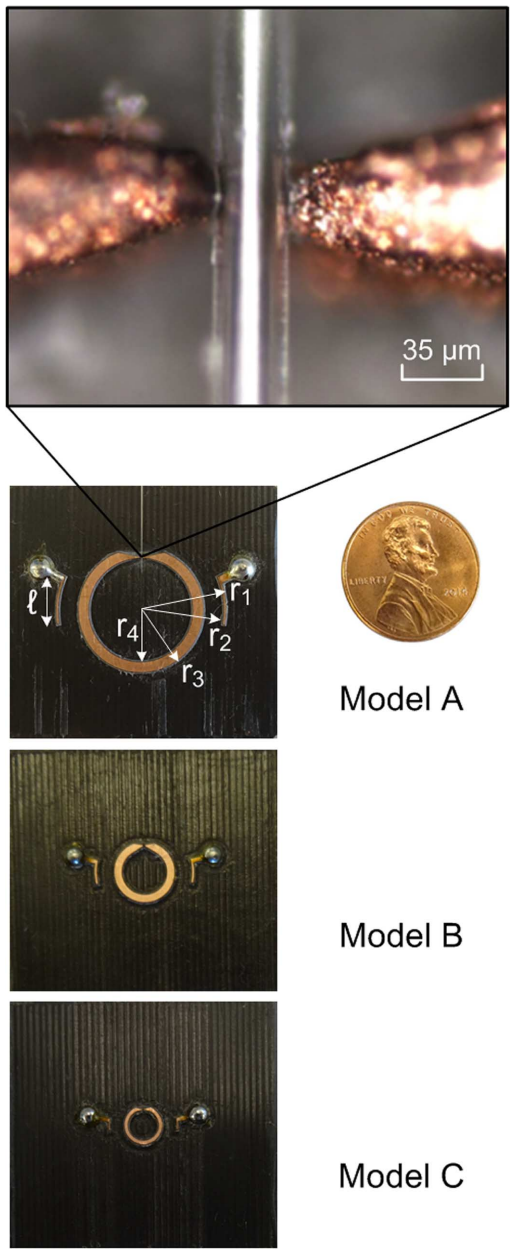

Fig. 7. Photographs of the fabricated sensors A-C, with a magnified view showing the position of the glass capillary within the gap region, model A given in [20].

2 mm was heated and then pulled down to an outer diameter of 34 μm and inner diameter of 30 μm in the case of the model A sensor. For the models B and C sensors, the inner and outer capillary diameters are 28 and 23 μm, respectively. Fig. 7 shows a photograph of the magnified gap region with the capillary, together with the layout for models A-C.

The constructional materials used here for the microwave microfluidic device comprised (i) an RT/duroid 5880 laminate, with (ii) an integrated soda glass capillary. The laminate was chosen because of its favorable dielectric properties due to its PTFE—glass-fiber construction. Whilst, the method used here for integrating the glass capillary and the circuit board, based split ring resonator, do not conform to currently used microfluidic mass-production techniques [27], the proof of principle functional operation does demonstrate that further work is justified in order to more effectively integrate the use of microwave interrogation techniques with microfluidic flows. The materials used to form microfluidic circuits depends hugely on the production volumes required, there disposability, solvent resistance, creep specifications, electro-optical transmission characteristics, and range from silicon, glasses, polymers, metals, elastomers, paper, sapphire, and diamond [28]. PTFE based materials, especially Teflon AF, do offer excellent dielectric properties, solvent resistance, and can be light transmissive, but equally are more difficult to bond as integrated capillary structures, and are not so amenable to cost-effective micro-structuring as is silicon and glass. It highly possible that the integrated microwave-microfluidic detectors, such as that demonstrated here, could be fabricated as a separate small-scale plug-in modules, that could be inserted within more complex electrofluidic motherboards, and that possibly the recent advances in additive 3D manufacturing [29] could enable such a hybrid assemblies made from diverse materials sets.

COMSOL Multiphysics 4.4 was used to perform 3D simulations of the electromagnetic fields of the sensors with and without polystyrene spheres in water at 25°C. The EM waves model was used to simulate the S-parameters of the SRRs. The wave equation in the frequency domain was computed in the EM waves model as described in the software according to

$$\nabla \times \mu_r^{-1}(\nabla \times \bar{E}) - k_o^2 \left(\varepsilon_r - \frac{j\sigma}{\omega \varepsilon_o}\right) \bar{E} = 0 \qquad (11)$$

where μ_r is the permeability, ε_r the permittivity and σ the electric conductivity of the material region; ε_o is the permittivity of the vacuum, k_o is the wave number in free space, and ω the angular frequency. The impedance boundary condition is used for the copper surfaces of the resonator and ground in order to incorporate the copper losses. The scattering boundary condition was utilized for the faces of the volume $40 \times 34 \times 40$ mm^3 (enclosing the device) to make the boundaries transparent for the scattered waves. Coaxial ports were used to feed the electromagnetic energy to the resonator. The relative permittivity of water ($\varepsilon = \varepsilon_1 - j\varepsilon_2$) was described in the simulation by using Debye Theory [30] as its permittivity is variable with frequency. The properties of the materials that were used in the simulation are shown in Table III. The simulated and measured results of the three models A- C are illustrated in Fig. 8. In Fig. 8 (a), the measured and simulated results of $|S_{21}|$ of the model A are shown for three cases: water only, water and 15 μm diameter microsphere, and water and 25 μm microsphere. The measured and simulated results of models B and C are illustrated in Fig. 8(b) and (c), respectively, for water and 15 μm diameter microsphere cases. In all models, the results shown in Fig. 8 demonstrate that there is good agreement between the measured and simulated results.

IV. Results and Discussion

A. Measurement Set-Up and Data for Sensor A

The bench-top assembly of the split ring resonator with the network analyzer, microscope and computer is shown in Fig. 9. We consider first the results of model A, with a resonance frequency of approximately 2.5 GHz. Fig. 10 shows the broadband transmission response (i.e., $|S_{21}|$) of the resonator's first

TABLE III
MATERIAL PROPERTIES USED IN THE SIMULATION AT 25° C

Material	ε_1	ε_2	σ (S/m)
Air	1	0	0
Microstrip Dielectric	2.21	0	3.17×10^{-4}
Copper	1	0	2.70×10^{7}
Polystyrene microsphere	2.10	0	0
Glass °apillary	3.80	0	1.00×10^{-12}
Water [31]	ε_s	ε_∞	τ (*p*se)
	78.4	5.16	8.27

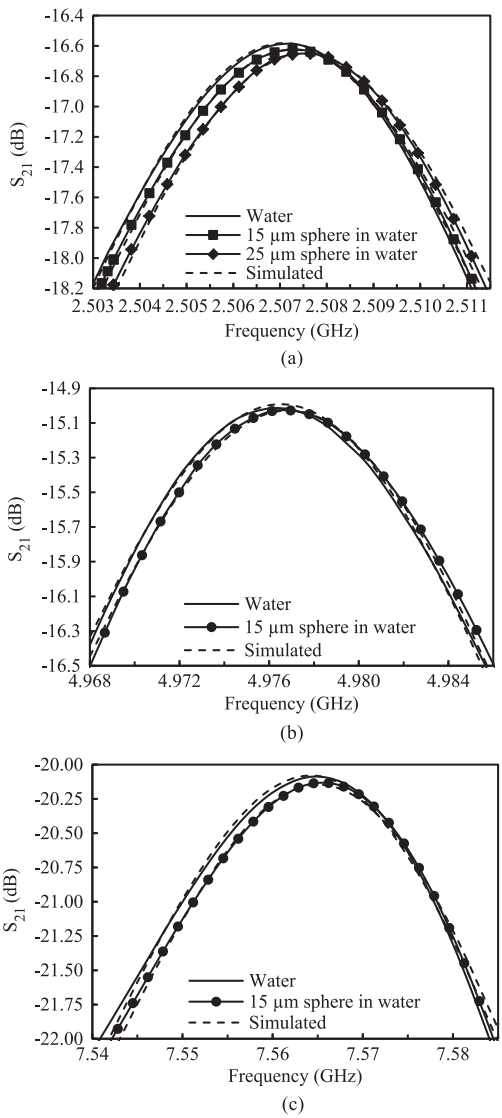

Fig. 8. Measured and simulated S_{21} of the sensors with a single microsphere dispersed in water in the gap region. (a) Model A, after [20]. (b) Model B. (c) Model C.

(odd mode) and second (even mode) resonance frequencies. The odd mode is perturbed by the dielectric properties of the material within the gap as there is a strong electric field there. Conversely, the even mode is almost unperturbed as its electric field is confined mostly between the ring and the ground plane.

Fig. 9. Photograph of the assembly of the sensor, network analyzer, laptop computer and optical microscope to aid positioning of the polystyrene microspheres in the gap region.

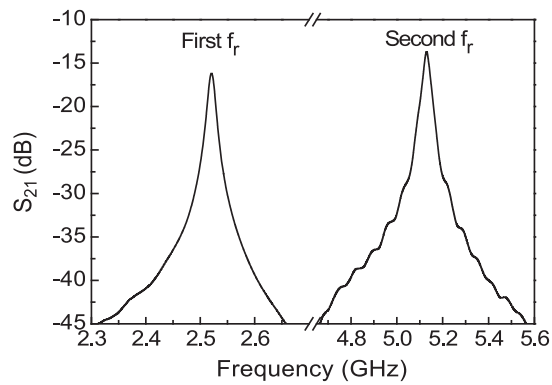

Fig. 10. Measured broadband $|S_{21}|$ response of the split ring resonator (model A) given in [20], showing the odd and even mode responses (the even mode has the higher frequency of the two).

The changes in the resonance frequency and the insertion loss of the odd mode with time due to a flow of microspheres along the capillary are shown in Fig. 11(a) and (b), respectively.

The results in Fig. 11 were collected by a computer running a LabView program to record instantaneously the change in resonance frequency and insertion loss of both modes owing to the movement of the microspheres. The $|S_{21}|$ data was fitted to a Lorentzian curve, from which the resonator parameters were extracted. The network analyzer was an Agilent E5071C, with an IF bandwidth of 10 kHz and 401 sweep points to give a sweep time of approximately 0.07 s. This is fast enough to capture enough data during the short time (around 2 s) when the microsphere occupied the gap region of the SRR. Increases in the odd mode resonance frequencies were measured to be 150 $\pm$ 8 kHz and 350 $\pm$ 18 kHz due to the presence of the 15 and 25 μm diameter microspheres, respectively. The increases in insertion loss were measured to be 0.030 $\pm$ 0.002 dB and 0.060 $\pm$ 0.003 dB, respectively. All errors quoted are random errors estimated from repeating each experiment three times. These dominate over other systematic errors linked to the measurement system.

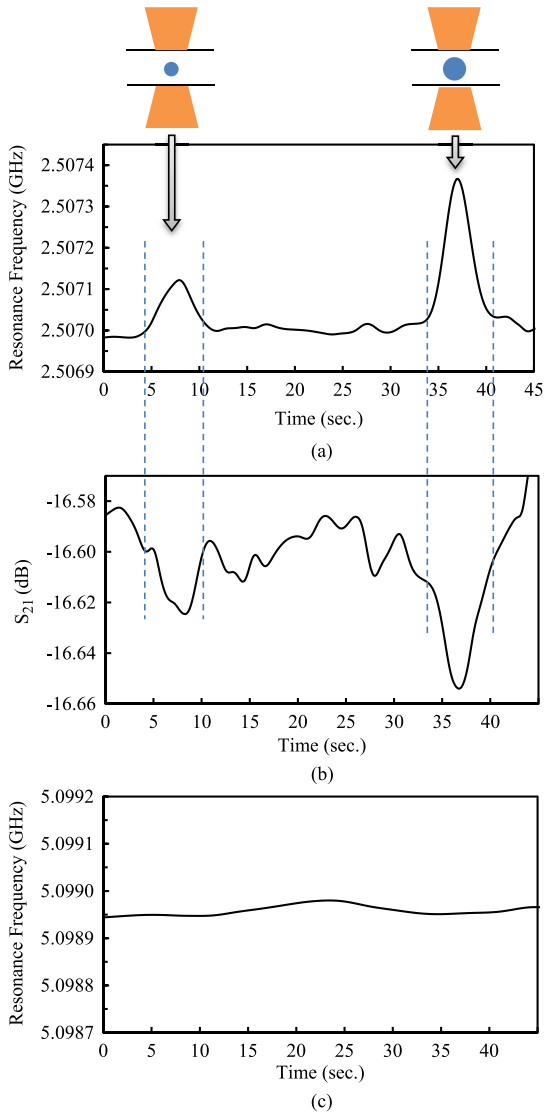

Fig. 11. Measured variation of the resonator parameters with respect to time when a 15 μm diameter microsphere enters the gap region of model A (2.5 GHz), followed by a 25 μm diameter microsphere, after [20]. (a) The resonance frequency of the odd mode, (b) the insertion loss of the odd mode, and (c) the resonance frequency of the even mode.

B. Use of the Even Mode and Effects of Changing Temperature

Furthermore, there was no measured perturbation of the even mode with the same microsphere flow, as expected (Fig. 11(c)). Therefore, the even mode has the very useful property that its resonance frequency can be used to monitor (and indeed correct for) minute changes in temperature. This is essential in a practical device owing to the highly temperature-dependent complex permittivity of water. Otherwise, small increases in temperature could be inferred as being due to changes in the dielectric properties of the microspheres. The complex permittivity of the microspheres can be extracted from the resonator measurements using approaches in [23] when the size of the microsphere is known. For example, in model A the extracted relative permittivity of microsphere is 2.1 $\pm$ 0.1.

Whilst the perturbations on the resonator are small in the case of Fig. 11, they can be unambiguously separated from the effects of small temperature changes. A change in temperature would cause the baseline to shift up or down, accordingly. However, this is likely to occur on a timescale which is much longer than the perturbations associated with the presence of the microspheres (typically less than 2 seconds), and these short term changes will be readily separated from the longer term effects of temperature drift.

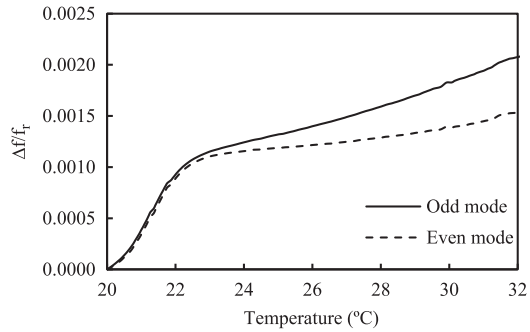

Fig. 12. Measured change in the fractional resonance frequency with temperature $\Delta f/f_r$ of both odd and even modes given in [20].

To verify the usefulness of the even mode in correcting for temperature, the sensor was measured in a temperature-controlled oven (Memmert, Model: IPP 400) with a high degree of temperature control ($\pm 0.1^{\circ}$C) over the range from 20 to 32°C. The resulting fractional changes in resonance frequencies of both modes with temperature are shown in Fig. 12. The resonance frequencies of both modes increase with temperature as the dielectric thickness expands with increasing temperature. The increase in frequency for the odd mode is some 30% larger than for the even mode due to additional expansion of the gap width, which causes an additional frequency shift. The results of Fig. 12 for the even mode can be used to deduce an accurate value of the temperature, and hence also the additional frequency shift in the odd mode caused by a change in temperature.

C. Use of Sensors B and C to Enhance Sensitivity

The increase in insertion loss when a microsphere is present is an interesting result that arises since the microsphere enhances the electric field inside the water filled capillary. This subsequently increases the dielectric losses, as has been discussed in detail in Section II-B.

To increase the ability of the sensor to discriminate the spheres with 15 μm diameter, or to deal with spheres (such as biological cells) which may not have such large differences in their permittivity with that of the host liquid, two smaller models B and C have been designed and tested.

In these two models the gap width was reduced to 30 μm and the ring radii were decreased to 3.5 and 2.25 mm for model B and C respectively, as shown in Table II. In model B, the resonance frequency is set at 5 GHz and its S_{21} is shown in Fig. 8(b). The changes in the resonance frequency and amplitude (losses) are shown in Fig. 13. The shift in resonance frequency is 400 $\pm$ 20 kHz and the increase in the insertion loss is 0.012 $\pm$ 0.001 dB, which is more sensitive to the 15 μm diameter microsphere than model A.

More sensitive results have been obtained from model C, as shown in Fig. 14. The shift in resonance frequency is now 1.00 $\pm$ 0.05 MHz and the increase of the insertion loss is 0.040 $\pm$

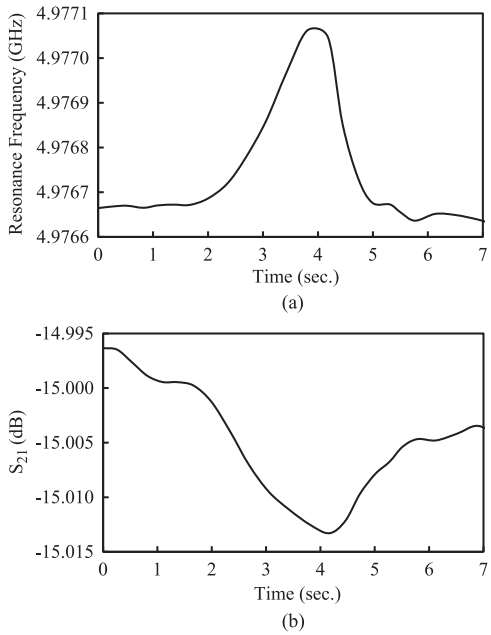

Fig. 13. Measured variation of the resonator parameters with respect to time when a 15 μm diameter microsphere enters the gap region in model B (5 GHz). (a) The resonance frequency (b) The insertion loss.

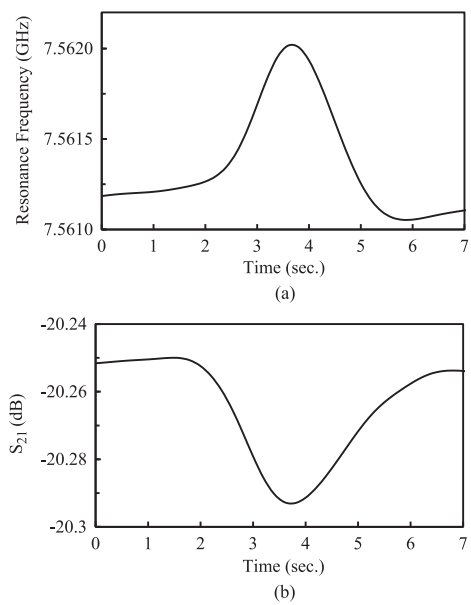

Fig. 14. Measured variation of the resonator parameters with respect to time when a 15 μm diameter microsphere enters the gap region in model C (7.5 GHz). (a) The resonance frequency (b) The insertion loss.

0.002 dB when the 15 μm diameter sphere passes though the model C's gap.

The results have some variation due to small temperature drifts. The change in temperature arises due to the flow of water inside the capillary; the water needs to reach thermal equilibrium to achieve stable, and hence accurate, results. In addition, the variation in results comes from the limitation of the network analyzer sensitivity as the changes in S_{21} are very small.

Finally, since we hope to apply our sensor for the detection of human cells, we have performed a simulation of the SRR with the 15 micron microsphere replaced by a "white blood cell" with diameter of 12 μm [16] of representative permittivity of 10 and conductivity of 0.5 at 7.5 GHz [32]. In the small SRR this gives a frequency shift of 0.5 MHz, so we expect our method to be able to quantify both the presence, and measure the complex permittivity, of individual cells.

V. Conclusion

In this work, three models of microwave sensors based on a microstrip split ring resonator were developed and tested for the dielectric measurement, size measurement and counting of microspheres. The high sensitivity of all three resonator models A-C is due to the small size of the gap region, here 35 and 30 μm. Two sizes of polystyrene microspheres (15 and 25 μm) have been used to verify the odd mode's perturbation when a microsphere is present in the gap. Furthermore, it has been demonstrated that the even mode is insensitive to the presence of microspheres and so can be used for temperature compensation. To increase the sensitivity as the real cell permittivity does not have large contrast with liquid permittivity, the gap and ring radii have been reduced in models B and C. Their increased sensitivity is simply due to the associated reduction in mode volume V_{m}. The observed changes in resonance frequency and insertion loss of the odd mode were due to the dielectric contrast between the microspheres and their host solvent (water). The complex permittivity of the microspheres can be extracted from the resonator measurements either using an optimization routine based on matching the simulated and experimental results or using the theoretical method in [23]. The ability of the split ring resonator sensor to count microspheres, as well as determine their complex permittivity, will next be applied to human cell detection and diagnostics.

References

[1] Y. Chen, H. Wu, Y. Hon, and H. Lee, "40 GHz RF biosensor based on microwave coplanar waveguide transmission line for cancer cells (HepG2) dielectric characterization," *Biosens. Bioelectron.*, vol. 61, pp. 417–421, Nov. 2014.

[2] T. Chen, F. Artis, D. Dubuc, J.-J. Fournié, M. Poupot, and K. Grenier, "Microwave biosensor dedicated to the dielectric spectroscopy of a single alive biological cell in its culture medium," in *Proc. IEEE MTT-S Int. Microw. Symp. Dig. (IMS)*, Seattle, WA, USA, Jun. 2–7, 2013, pp. 1–4.

[3] F. Artis, D. Dubuc, J.-J. Fournié, M. Poupot, and K. Grenier, "Microwave dielectric spectroscopy of cell membrane permeabilization with saponin on human B lymphoma cells," in *Proc. IEEE MTT-S Int. Microw. Symp. Dig. (IMS)*, Tampa, FL, USA, Jun. 1–6, 2014, pp. 1–4.

[4] C. Dalmay, A. Pothier, P. Blondy, F. Lalloue, and M.-O. Jauberteau, "Label free biosensors for human cell characterization using radio and microwave frequencies," in *Proc. IEEE MTT-S Int. Microw. Symp. Dig. (IMS)*, Atlanta, GA, USA, Jun. 15–20, 2008, pp. 911–914.

[5] A. Landoulsi, L. Y. Zhang, C. Dalmay, A. Lacroix, A. Pothier, A. Bessaudou, P. Blondy, S. Battu, F. Lalloué, C. B. MdP, and C. Lautrette, "Tunable frequency resonator biosensors dedicated to dielectric permittivity analysis of biological cell cytoplasm," in *Proc. IEEE MTT-S Int. Microw. Symp. Dig. (IMS)*, Seattle, WA, USA, Jun. 2–7, 2013, pp. 1–4.

[6] M. S. Boybay, A. Jiao, T. Glawdel, and C. L. Ren, "Microwave sensing and heating of individual droplets in microfluidic devices," *Lab Chip*, vol. 13, no. 19, pp. 3840–3846, Oct. 2013.

[7] C. Dalmay, A. Pothier, P. Blond, M. Cheray, F. Lalloue, and M.-O. Jauberteau, "RF biosensor based on microwave filter for biological cell characterisation," in *Proc. Eur. Microw. Conf. (EuMC)*, Rome, Sep. 29–Oct. 1 2009, pp. 41–44.

[8] Y. Yang, Y. He, H. Zhang, K. Huang, G. Yu, and P. Wang, "Measuring the microwave permittivity of single particles," in *Proc. 2013 IEEE Topical Conf. Biomed. Wireless Technologies, Networks, Sensing Systems (BioWireleSS)*, Austin, TX, USA, Jan. 20–23, 2013, pp. 28–30.

[9] Y. Yang, H. Zhang, J. Zhu, G. Wang, T.-R. Tzeng, X. Xuan, K. Huang, and P. Wang, "Distinguishing the viability of a single yeast cell with an ultra-sensitive radio frequency sensor," *Lab on a Chip*, vol. 10, pp. 553–555, Mar. 2010.
[10] G. A. Ferrier, S. F. Romanuik, D. J. Thomson, G. E. Bridges, and M. R. Freeman, "A microwave interferometric system for simultaneous actuation and detection of single biological cells," *Lab on a Chip*, vol. 9, pp. 3406–3412, Dec. 2009.
[11] J. Wessel, K. Schmalz, J. C. Scheytt, B. Cahill, and G. Gastrock, "Microwave biosensor for characterization of compartments in teflon capillaries," in *Proc. Eur. Microw. Conf. (EuMC)*, Oct. 29–Nov. 1 2012, pp. 534–537.
[12] Y. Ning, C. Multari, X. Luo, C. Palego, X. Cheng, J. C. M. Hwang, A. Denzi, C. Merla, F. Apollonio, and M. Liberti, "Broadband electrical detection of individual biological cells," *IEEE Trans. Microw. Theory Tech.*, vol. 62, no. 9, pp. 1905–1911, Sep. 2014.
[13] A. Denzi, F. Apollonio, M. Liberti, M. Caterina, Y. Ning, C. Multari, C. Palego, X. Cheng, and J. C. M. Hwang, "Cell detection and discrimination by a microfluidic-integrated broadband microchamber," in *Proc. Eur. Microw. Conf. (EuMC)*, Rome, Oct. 6–9, 2014, pp. 695–698.
[14] D. Dubuc, O. Mazouffre, C. Llorens, T. Taris, M. Poupot, J.-J. Fournié, J.-B. Begueret, and K. Grenier, "Microwave-based biosensor for on-chip biological cell analysis," *Analog Integr. Circuits Signal Process*, vol. 77, pp. 135–142, Nov. 2013.
[15] M. Nikolic-Jaric, S. F. Romanuik, G. A. Ferrier, G. E. Bridges, M. Butler, K. Sunley, D. J. Thomson, and M. R. Freeman, "Microwave frequency sensor for detection of biological cells in microfluidic channels," *Biomicrofluidics*, vol. 3, no. 3, p. 034103, Sep. 2009.
[16] Y. Polevaya, I. Ermolina, M. Schlesinger, B.-Z. Ginzburg, and Y. Feldman, "Time domain dielectric spectroscopy study of human cells II. Normal and malignant white blood cells," *Biochimica et Biophysica Acta*, vol. 1419, pp. 257–271, Jul. 1999.
[17] Q. Hu, R. P. Joshi, and A. Beskok, "Model study of electroporation effects on the dielectrophoretic response of spheroidal cells," *J. Appl. Phys.*, vol. 106, no. 2, p. 024701, Jul. 2009.
[18] L. L. Sohn, O. A. Saleh, G. R. Facer, A. J. Beavis, R. S. Allan, and D. A. Notterman, "Capacitance cytometry: Measuring biological cells one by one," *Proc. Nat. Acad. Sci. United States of America (PNAS)*, vol. 97, no. 20, pp. 10687–10690, Sep. 2000.
[19] K. Asami, "Characterization of biological cells by dielectric spectroscopy," *J. Non-Crystalline Solids*, vol. 305, no. 1–3, pp. 268–277, Jul. 2002.
[20] A. Abduljabar, X. Yang, D. Barrow, and A. Porch, "Microstrip Split Ring Resonator for Microsphere Detection and Characterization," in *Proc/ IEEE MTT-S Int. Microw. Symp. Dig. (IMS)*, Phoenix, AZ, USA, May 17–22, 2015, pp. 1–4.
[21] J. Chen, L. Quyen, and X. Zhu, "Loss compensated high- tunable bass-pass filter usingmicrostrip ring resonators," in *Proc. Int. Conf. Adv. Technol. Commun.*, Da Nang, Aug. 2–4, 2011, pp. 191–194.
[22] K. Chang and L.-H. Hsieh, *Microwave Ring Circuits and Related Structures*, 2nd ed. New York, NY, USA: Wiley, 2004.
[23] A. A. Abduljabar, D. J. Rowe, A. Porch, and D. A. Barrow, "Novel microwave microfluidic sensor using a microstrip split-ring resonator," *IEEE Trans. Microw. Theory Tech.*, vol. 62, no. 3, pp. 679–688, Mar. 2014.
[24] D. M. Pozar, *Microwave Engineering*. New York, NY, USA: Wiley, 2005.
[25] A. Masood, A. Porch, and D. Barrow, *Microwave Resonators for Highly Sensitive Compositional Analysis*. Saarbrücken, Germany: LAMBERT, 2010.
[26] D. J. Rowe, S. al-Malki, A. A. Abduljabar, A. Porch, D. A. Barrow, and C. J. Allender, "Improved split-ring resonator for microfluidic sensing," *IEEE Trans. Microw. Theory Tech.*, vol. 62, no. 3, pp. 689–699, Mar. 2014.
[27] Y. Temiz, R. D. Lovchik, G. V. Kaigala, and E. Delamarche, "Lab-on-a-chip devices: How to close and plug the lab?," *Microelectronic Eng.*, vol. 132, pp. 156–175, Jan. 2015.
[28] K. Ren, J. Zhou, and H. Wu, "Materials for microfluidic chip fabrication," *Acc. Chem. Res.*, vol. 46, no. 11, pp. 2396–2406, Jun. 2013.
[29] S. Gowers, V. F. Curto, C. A. Seneci, C. Wang, S. Anastasova, P. Vadgama, G. Yang, and M. Boutelle, "3D printed microfluidic device with integrated biosensors for online analysis of subcutaneous human microdialysate," *Anal. Chem.*, vol. 87, no. 15, pp. 7763–7770, Aug. 2015.
[30] H. Frohlich, *Theory of Dielectrics*. New York, NY, USA: Oxford Univ. Press, 1958.
[31] F. Buckley and A. A. Maryott, "Tables of dielectric dispersion data for pure liquids and dilute solutions," *Nat. Bureau Standards Circular*, vol. 589, p. 6, Nov. 1958.
[32] S. Abdalla, "Complex permittivity of blood cells E.coli suspensions," *J. Molecular Liq.*, vol. 160, no. 3, pp. 130–135, May 2011.

Ali A. Abduljabar (S'14) received the B.Sc. and M.Sc. degrees in electrical engineering from University of Basrah, Basrah, Iraq. He is currently working toward the Ph.D. degree at Cardiff University, Cardiff, U.K.

He was a Lecturer in wireless and microwave communications engineering with the University of Basrah, Basrah, Iraq. His research concerns the design of microwave sensors and microwave heating techniques for microfluidic systems and non-invasive applications.

Xin Yang received the B.Sc. degree in biomedical engineering from Beijing Jiaotong University, China, and the M.Sc. degree in medical electronics and physics from Queen Mary, University of London, U.K., and Ph.D. degree in medical engineering from Cardiff University, Cardiff, U.K.

He is a Lecturer in medical electronics with the School of Engineering, Cardiff University, who has a background in the medical instrumentation and medical ultrasound. He has been exploring innovative techniques including microwave, electrical and optical methods in cancer detection and diagnosis. Much of his research is multidisciplinary, with collaborations with University Hospital Wales, Cardiff School of Medicine and Dentistry. He has published papers in the field of clinical and preclinical ultrasound, and eight textbooks in electronics.

David A. Barrow received the B.Sc. (hons.) degree in biological sciences and the Ph.D. degree in ecological sciences from the University of Wales, Cardiff, U.K.

He is a multidisciplinary Scientist and Professor of microfluidics at Cardiff University School of Engineering, He has researched a diversity microfluidic-based phenomena and devices, including chemical sensors, porous silicon, microacoustics, hybrid integration, micromolding, emulsion and digital microfluidics, chemical separations, plasma etching, CFD, microwave sensors, laser micromachining, and marine microanalysis systems. He was a founder of the metaFAB TSB open-access NanoCentre, MSTB Ltd., researching space microsystems, Protasis Corporation, developing microdevices for chemical separations, and Q-CHIP Ltd., developing injectable microencapsulated pharmaceuticals. He currently researchers the fabrication of nuclear fusion targets, artificial cells and stem cell microcapsules.

Adrian Porch received the M.A. degree in physics and Ph.D. degree in low-temperature physics from Cambridge University, Cambridge, U.K.

He is a Professor with the School of Engineering, Cardiff University, Cardiff, U.K., and a member of the Centre for High Frequency Engineering. He is also Deputy Director of School, responsible for Research and Innovation. He has over 25 years of experience in applying microwave methods to measure and understand the fundamental properties of electronic materials. More recently, his techniques have been used to develop new types of electromagnetic sensors, with emphasis on applications across different disciplines.